The Contribution of Radiative Feedbacks to Orbitally Driven Climate Change

MICHAEL P. ERB AND ANTHONY J. BROCCOLI

Department of Environmental Sciences, Rutgers, The State University of New Jersey, New Brunswick, New Jersey

AMY C. CLEMENT

Rosenstiel School of Marine and Atmospheric Science, University of Miami, Miami, Florida

(Manuscript received 2 July 2012, in final form 5 February 2013)

ABSTRACT

Radiative feedbacks influence Earth's climate response to orbital forcing, amplifying some aspects of the response while damping others. To better understand this relationship, the GFDL Climate Model, version 2.1 (CM2.1), is used to perform idealized simulations in which only orbital parameters are altered while ice sheets, atmospheric composition, and other climate forcings are prescribed at preindustrial levels. These idealized simulations isolate the climate response and radiative feedbacks to changes in obliquity and longitude of the perihelion alone. Analysis shows that, despite being forced only by a redistribution of insolation with no global annual-mean component, feedbacks induce significant global-mean climate change, resulting in mean temperature changes of −0.5 K in a lowered obliquity experiment and +0.6 K in a NH winter solstice perihelion minus NH summer solstice perihelion experiment. In the obliquity experiment, some global-mean temperature response may be attributable to vertical variations in the transport of moist static energy anomalies, which can affect radiative feedbacks in remote regions by altering atmospheric stability. In the precession experiment, cloud feedbacks alter the Arctic radiation balance with possible implications for glaciation. At times when the orbital configuration favors glaciation, reductions in cloud water content and low-cloud fraction partially counteract changes in summer insolation, posing an additional challenge to understanding glacial inception. Additionally, several systems, such as the Hadley circulation and monsoons, influence climate feedbacks in ways that would not be anticipated from analysis of feedbacks in the more familiar case of anthropogenic forcing, emphasizing the complexity of feedback responses.

1. Introduction

Paleoclimate modeling and data studies suggest that large periodic variations in past global-mean temperature have been driven by cyclical changes in Earth's eccentricity, obliquity, and longitude of the perihelion. By dictating the earth's orbital geometry, these three cycles alter the seasonal and latitudinal distribution of insolation, which (amplified by internal climate system feedbacks) can result in global-mean climate change. The idea that orbital cycles are responsible for glacial–interglacial cycles and other Quaternary variations was championed by Milankovitch (1941) and has since been expanded in work by Hays et al. (1976) and numerous others in more recent times (e.g., Imbrie et al. 1993; Raymo and Nisancioglu 2003). For glacial–interglacial cycles, low obliquity (axial tilt) and Northern Hemisphere (NH) winter solstice perihelion encourage ice sheet expansion by reducing NH summer insolation. This orbital theory suggests that by allowing ice to survive through the less intense melt season, additional ice may accumulate during the winter, cooling the earth through a positive ice–albedo feedback.

Orbital signals in the proxy record have been well documented (e.g., Petit et al. 1999; Jouzel et al. 2007), but uncertainties remain concerning the exact climatic effects of orbital forcing. Hypotheses have been proposed to answer unresolved questions such as why climate variations dominantly occur with 100-kyr periodicity in the late Pleistocene (Imbrie et al. 1993; Huybers 2006) and why 40 kyr is the dominant period in the early Pleistocene (Raymo and Nisancioglu 2003; Huybers 2006; Huybers and Tziperman 2008). Because global annual-mean

Corresponding author address: Michael P. Erb, Department of Environmental Sciences, Rutgers, The State University of New Jersey, 14 College Farm Road, New Brunswick, NJ 08901.
E-mail: mperb@envsci.rutgers.edu

DOI: 10.1175/JCLI-D-12-00419.1

radiative forcing caused by orbital cycles is exceedingly small, substantial climate feedbacks are necessary to explain global-mean climate shifts.

General circulation models provide a useful way to investigate the role of feedbacks in orbitally forced climate change. While much focus in modeling has been placed on specific time periods such as the last glacial maximum, last interglacial, and the mid-Holocene, attribution of the influence of orbital signals in such simulations is complicated by competing effects from changes in ice sheets and atmospheric composition. Idealized simulations in which only the orbital configuration is changed can provide a clearer picture of the feedback response.

Several studies using idealized simulations have already been completed, with early work being done by Phillipps and Held (1994), who investigated the climate response under various orbital configurations. More recently, Jackson and Broccoli (2003) ran an atmosphere–slab ocean model forced with only the accelerated orbital forcing of the past 165 kyr and found that low obliquity and late NH spring aphelion led to enhanced snow accumulation at times mostly consistent with the proxy record, largely influenced by storm activity and feedbacks involving sea ice. Further analysis highlighted the importance of atmospheric dynamics such as the northern annular mode (Hall et al. 2005). Other idealized orbital forcing studies have focused on the roles of vegetation and sea ice (Tuenter et al. 2005a,b), the effect of precession at the last interglacial (Khodri et al. 2005), the response of the tropical climate to orbital forcing (Clement et al. 2004; Lee and Poulsen 2005; Timmermann et al. 2007), the response of monsoons to orbital forcing (Wyrwoll et al. 2007), and feedbacks in response to changes in obliquity (Lee and Poulsen 2008; Mantsis et al. 2011).

In this study, a fully coupled atmosphere–ocean general circulation model (AOGCM) is employed to further explore the role of feedbacks in orbitally forced climate simulations. While there have been other studies that look at the climate response to orbital cycles, little focus has been placed on the role of radiative feedbacks, particularly with a fully coupled AOGCM. In addition, a novel aspect of this research is the use of the kernel method of feedback analysis, which has rarely been applied to paleoclimate simulations. Another novel aspect of this research is the idealized experimental design, in which the climate response to changes in obliquity and longitude of the perihelion may be isolated and explored.

To better understand the feedback response, feedbacks computed in these orbital experiments are also compared with feedbacks from a doubled CO_2 experiment. Previous studies have suggested that feedbacks operate similarly in simulations driven by changes in different forcing agents (e.g., CO_2, solar irradiance, and organic carbon), although the feedbacks do show some sensitivity to the latitude and altitude of the imposed forcing (Yoshimori and Broccoli 2008). The comparison of feedbacks under orbital and anthropogenic forcing in the present paper provides a test of this idea and will allow us to identify which aspects of feedback remain consistent under different forcings, and which are sensitive to the type and distribution of forcing.

TABLE 1. Orbital values for obliquity and precession simulations. Obliquity simulations (Hi and Lo) represent the high and low obliquity of the past 600 kyr (Berger and Loutre 1991). Precession simulations (WS and SS) represent opposite times on the precession cycle, with increased eccentricity to amplify the signal. Numbers in italics are preindustrial values.

Simulation Name	Eccentricity	Lon of perihelion (°)	Obliquity (°)
Lo	*0.01671*	*102.932*	22.079
Hi	*0.01671*	*102.932*	24.480
WS	0.0493	90	*23.439*
SS	0.0493	270	*23.439*

The design of the orbital forcing experiments is outlined in section 2. Section 3 explores the temperature response in these orbital experiments. The roles of feedbacks in producing the modeled climate change are discussed in section 4, and section 5 compares feedbacks under orbital forcings to those under anthropogenic forcing. Section 6 considers the potential effect of cloud feedbacks on large-scale NH ice sheet growth, and the paper's conclusions are stated in section 7.

2. Experimental design

The AOGCM used for this study is the Geophysical Fluid Dynamics Laboratory (GFDL) Climate Model, version 2.1 (CM2.1), which has atmosphere, ocean, land, and sea ice components coupled without flux adjustments. Atmospheric resolution is 2° latitude by 2.5° longitude with 24 vertical levels, and ocean resolution is 1° by 1°, becoming finer in the tropics to a meridional resolution of ⅓° with 50 vertical levels (Delworth et al. 2006). Reichler and Kim (2008) compared simulations of preindustrial climate and found that CM2.1 performed the best among the models from phase 3 of the Coupled Modeling Intercomparison Project (CMIP3).

To explore feedback mechanisms under obliquity- and precession-only forcing, four idealized equilibrium simulations have been conducted (Table 1). For obliquity, two simulations set obliquity to the low (22.079°) and high (24.480°) extremes of the past 600 kyr with all other variables, such as ice sheet extent and atmospheric

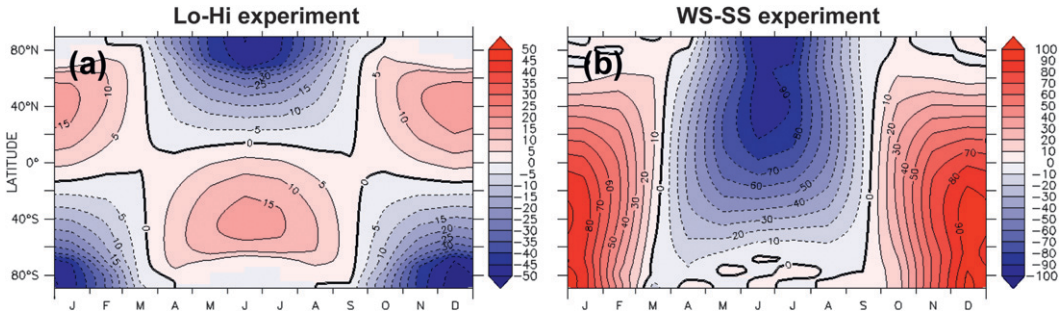

FIG. 1. Seasonal changes in zonal-mean insolation ($W\,m^{-2}$) for the (a) Lo–Hi and (b) WS–SS experiments as a function of latitude.

composition, prescribed at preindustrial levels. To isolate precession, two simulations set perihelion to the NH winter solstice (WS) and NH summer solstice (SS) with all other variables prescribed to preindustrial levels except eccentricity, which is increased to 0.0493, the maximum eccentricity of the past 600 kyr (Berger and Loutre 1991). Because the effects of precession on insolation scale with eccentricity, this value of eccentricity has been chosen to raise the signal-to-noise ratio in the precession results. A CMIP3 (Meehl et al. 2007) doubled CO_2 simulation, in which CO_2 is increased from preindustrial levels at 1% yr^{-1} until doubling and stabilized at that level thereafter (Stouffer et al. 2006), is compared with a preindustrial control run. This doubled CO_2 experiment is used as the basis for comparing feedbacks under orbital forcing with those estimated from anthropogenic forcing. Because CM2.1 lacks dynamic ice sheets, dynamic vegetation, and a carbon cycle, the analysis in this paper focuses on the fast radiative feedbacks in the climate system (i.e., surface albedo, water vapor, lapse rate, and clouds).

In the precession results, a calendar adjustment has been made. Because of the elliptical shape of Earth's orbit, changes in longitude of the perihelion alter the lengths of seasons according to Kepler's second law. When comparing precession results on a standard fixed-day calendar, this causes dates to become offset from each other, making comparison between simulations problematic (Joussaume and Braconnot 1997). As a remedy for this problem, precession results have been converted to a common fixed-angular calendar where each ''month'' corresponds to a 30° arc of orbit. The conversion was made using the method outlined in Pollard and Reusch (2002), which is one of several proposed methods (Timm et al. 2008; Chen et al. 2010).

All of the orbital forcing simulations were run for 600 years, and the results presented in this paper use the mean of years 501–600. The precession simulations were run on a slightly updated version of CM2.1, which implements some bug fixes and has a slightly different value for snow albedo as well as some other minor changes, but these adjustments do not appear to affect the results. For analysis purposes, results of the orbital forcing simulations are presented as low minus high obliquity (the Lo–Hi experiment) and NH winter solstice perihelion minus NH summer solstice perihelion (the WS–SS experiment). This convention is undertaken so both experiments reduce the NH summer insolation, which is conducive to NH glaciation.

The Lo–Hi experiment discussed in this paper has also been analyzed in Mantsis et al. (2011), which uses two different methods to investigate feedbacks in response to obliquity changes. The present paper expands upon the work of Mantsis et al. (2011) by exploring feedbacks computed with the kernel method in greater depth, with a focus on the physical mechanisms that lead to the feedback responses. The climate response and feedbacks in the WS–SS experiment have not been previously explored.

3. Insolation change and temperature response

The Lo–Hi experiment is defined by a decrease in Earth's axial tilt from 24.480° to 22.079°. In an annual-mean sense, this increases top-of-atmosphere (TOA) solar radiation in the tropics by several watts per square meter and decreases it at higher latitudes by up to $\sim 15\,W\,m^{-2}$, increasing the equator-to-pole insolation gradient (Fig. 1a). Seasonally, the amplitude of the extratropical insolation cycle is reduced in both hemispheres—winter insolation increases by over $15\,W\,m^{-2}$ and summer insolation decreases by up to $\sim 50\,W\,m^{-2}$. In comparison, the WS–SS experiment consists of changing Earth's perihelion from NH summer solstice to NH winter solstice, resulting in increased insolation during the half year centered on NH winter solstice and decreased insolation for the rest of the year, with monthly insolation differences as large as $\sim 100\,W\,m^{-2}$ (Fig. 1b). The WS–SS insolation anomalies reach their peak in mid- and high-latitude summer when the magnitude of insolation

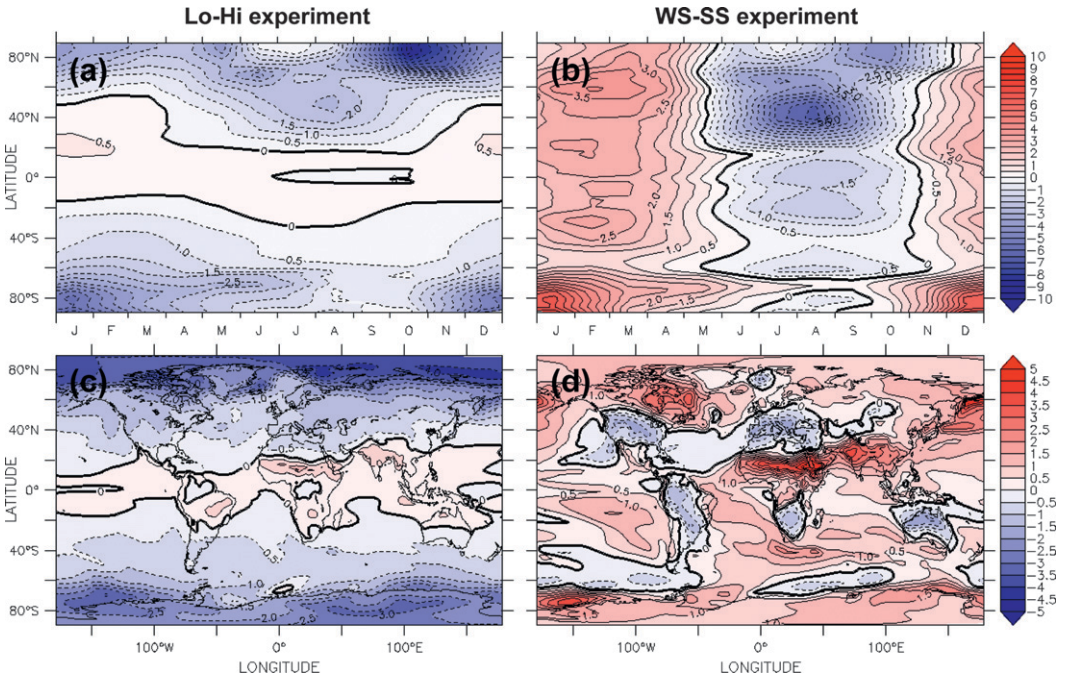

FIG. 2. Change in (a),(b) zonal-mean surface air temperature (K) and (c),(d) annual-mean surface air temperature (K) for the (left) Lo–Hi and (right) WS–SS experiments.

is largest and result in a weakening of the NH but a strengthening of the Southern Hemisphere (SH) annual insolation cycle.

Responding to these changes, the seasonal- and annual-mean surface air temperature changes ΔT are shown for both experiments in Fig. 2. The Lo–Hi experiment exhibits a slightly positive ΔT throughout most of the tropics, averaging +0.1 K over the tropics, with decreases in ΔT over the mid- and high latitudes becoming greater in magnitude toward the poles. In the midlatitudes, winter ΔT is mostly negative despite positive insolation changes during that season. This is because of the large heat capacity of the upper ocean, which acts as an integrator of forcing. On the whole, the equator-to-pole temperature gradient is increased. Other features of the temperature response are discussed in Mantsis et al. (2011). Importantly, negative annual-mean ΔT extends equatorward of negative annual-mean insolation change, suggesting that feedbacks can overwhelm the direct effects of local insolation forcing.

In the WS–SS experiment, ΔT exhibits much more seasonal variation, with most latitudes experiencing negative ΔT from approximately June to October and positive ΔT through the rest of the year, which is delayed from the insolation changes by as much as several months because of the thermal inertia of the climate system. In Antarctica, which is more thermally isolated by virtue of the Antarctic Circumpolar Current, ΔT remains positive through almost all of the year. Spatially, annual-mean ΔT is especially positive over the North African and Indian Ocean monsoon regions, with negative ΔT mostly confined to midlatitude continents. The reasons for these changes are explored in the following section.

In both the Lo–Hi and WS–SS experiments, global annual-mean insolation change is zero. A more accurate measure of the change in insolation felt by the climate system is radiative forcing, which is defined by Ramaswamy et al. (2001) as "the change in net (down minus up) irradiance (solar plus long-wave; in W m^{-2}) at the tropopause after allowing for stratospheric temperatures to readjust to radiative equilibrium, but with surface and tropospheric temperatures and state held fixed at the unperturbed values." In the present paper, radiative forcing does not include longwave radiation, and stratospheric temperatures are not allowed to adjust. Positive values of radiative forcing represent a heating of the climate system. Despite the absence of a net change in global annual-mean insolation, mean radiative forcing is +0.10 W m^{-2} for Lo–Hi and −0.11 W m^{-2} for WS–SS because of the spatial and temporal covariance of insolation anomalies and albedo. Although the radiative forcing is small, global-mean ΔT is −0.5 K for Lo–Hi and +0.6 K for WS–SS. This disproportionate ΔT response (which is opposite to the sign of the radiative forcing in both cases) indicates the crucial role of radiative feedbacks in determining climate response to orbital forcing.

4. Radiative feedbacks

The ''fast'' radiative feedbacks, which are the focus of this research, involve changes in Earth's surface albedo α_s, atmospheric water vapor q, vertical temperature lapse rate Γ, and cloud optical properties c. These four radiative feedbacks, plus the blackbody sensitivity $\delta F/\delta T$, equal the total climate sensitivity dF/dT (which is the change in radiative forcing per unit temperature change) in CM2.1, as expressed in the following equation:

$$\frac{dF}{dT} = \frac{\delta F}{\delta T} + \frac{\delta F}{\delta \alpha_s}\frac{\delta \alpha_s}{\delta T} + \frac{\delta F}{\delta q}\frac{\delta q}{\delta T} + \frac{\delta F}{\delta \Gamma}\frac{\delta \Gamma}{\delta T} + \frac{\delta F}{\delta c}\frac{\delta c}{\delta T}.$$

In the absence of vegetation and geological changes, changes in surface albedo result from variations in sea ice and continental snow cover, which tend to enhance climate perturbations through melt or expansion. Water vapor is an effective greenhouse gas, so its concentration and distribution influence the atmosphere's ability to affect longwave (LW) radiation and, to a smaller extent, shortwave (SW) radiation. A change in the lapse rate (the rate at which temperature decreases with height) affects the loss of LW radiation to space by affecting the emitting temperature of the upper troposphere, which emits to space more readily than the surface. Clouds affect the radiation balance through the absorption and scattering of SW radiation and the absorption and emission of LW radiation in the atmosphere, so changes in the amount, distribution, and water content of clouds may amplify or diminish climate perturbations.

To isolate and quantify these feedbacks, the kernel method outlined in Soden and Held (2006) and Soden et al. (2008) is employed. This method uses a set of radiative ''kernels,'' computed using a stand-alone radiation code to quantify the net changes in TOA radiation that result from unit changes in surface albedo, water vapor, and lapse rate at each grid point and time of year. The cloud feedback cannot be calculated explicitly with this method because of strong nonlinearities in the cloud feedback, but is instead calculated by adjusting the change in cloud radiative forcing to account for the influence of clouds in masking noncloud feedbacks (i.e., temperature, water vapor, and surface albedo; Soden et al. 2004, 2008). The kernel method is convenient because it can differentiate the effects of concurrent radiative feedbacks without the need to rerun model code, which can be computationally expensive. In interpreting the following results it should be noted that the results are here expressed as the effect of feedbacks on net TOA radiation ΔR_{net} ($\mathrm{W\,m^{-2}}$), rather than as feedbacks ($\mathrm{W\,m^{-2}\,K^{-1}}$). Doing so avoids dividing by the small values of global-mean ΔT in the orbital experiments. Positive values of ΔR_{net} indicate increased net downward radiation. In the following subsections the role of each feedback under orbital forcing is examined. A further analysis of some of the mechanisms at work will follow in section 5.

a. Surface albedo feedback

The ΔR_{net} from the surface albedo feedback is shown in Figs. 3a and 3b. In the Lo–Hi experiment, the sea ice fraction increases in the Arctic Ocean, Greenland Sea, Barents Sea, and Bering Sea, and snow cover increases across much of the NH high-latitude continents, increasing reflection of SW radiation primarily in the NH summer when insolation values are high. SH changes are characterized by increases in sea ice in much of the Southern Ocean, but snow expansion is limited by a lack of SH midlatitude continental areas and by the thermal isolation of Antarctica, which sustains snow cover yearround, causing SH changes to be less extensive than NH ones. Global-mean ΔR_{net} for each feedback is given in Table 2. The global-mean ΔR_{net} from the surface albedo feedback in the Lo–Hi experiment is $-0.27\,\mathrm{W\,m^{-2}}$, indicating a cooling effect.

In the WS–SS experiment, snow and sea ice changes occur in largely the same regions as the Lo–Hi experiment, but present a more seasonally varying response because of the more seasonal nature of the forcing. In the NH, snow cover retreats more during a warmer NH spring and Arctic sea ice retreats less during a cooler NH summer. Aided by the large size of NH midlatitude continents, snow retreat has a larger total effect on albedo than sea ice increase, so the total effect of these two competing NH changes is a warming. In the SH, Southern Ocean sea ice retreats farther than normal during the warmer SH summer. However, because of the limited area of SH midlatitude continents, SH snow cover anomalies during SH spring are small despite cooler temperatures. This imbalance in the land–sea distribution allows sea ice reductions to dominate the SH albedo response, leading to a warming effect. Global-mean ΔR_{net} from the surface albedo feedback is $+0.31\,\mathrm{W\,m^{-2}}$ in the WS–SS experiment, emphasizing the importance of seasonality and surface type in determining feedback responses.

b. Water vapor feedback

The ΔR_{net} from the water vapor feedback is given in Figs. 3c and 3d and is characterized by both latitudinal and seasonal variations for Lo–Hi and mostly seasonal variations for WS–SS, generally having a warming effect where ΔT is positive and a cooling effect where ΔT is negative. To see what effect circulation changes have on this feedback, the water vapor response is separated into two components (Fig. 4): a thermodynamic component

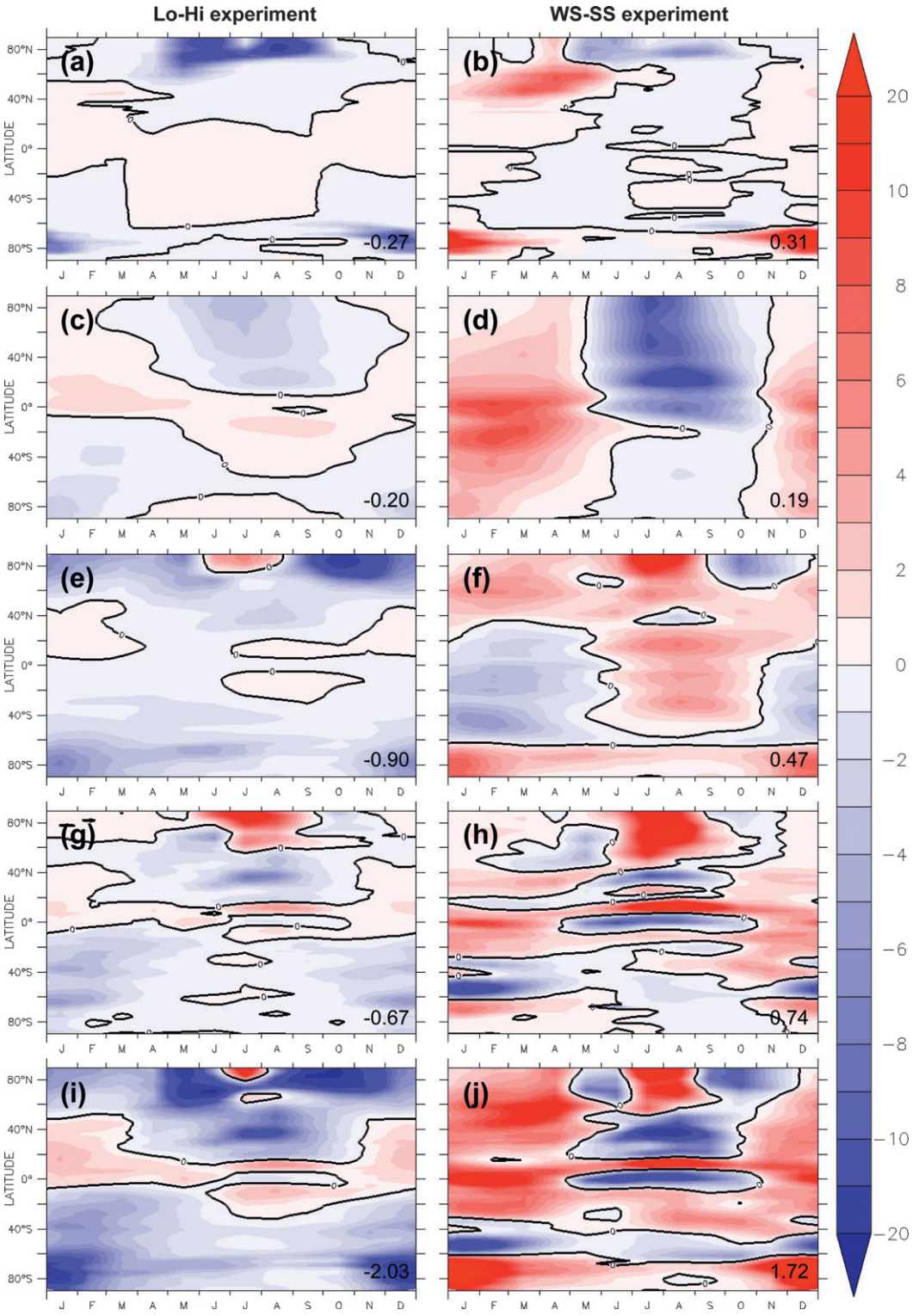

FIG. 3. Effect of feedbacks on zonal-mean ΔR_{net} (W m^{-2}) caused by (a),(b) surface albedo, (c),(d) water vapor, (e),(f) lapse rate, (g),(h) clouds, and (i),(j) the sum of all four for the Lo–Hi and WS–SS experiments, respectively. Positive values represent increased net downward radiation. Global-mean values (W m^{-2}) are given in the bottom right of each panel.

TABLE 2. Global annual-mean values for the effect of each feedback on ΔR_{net} (W m^{-2}). Estimated values, which are discussed in section 5, are given in parentheses for the sake of comparison. Note that different lengths of months between NH winter and NH summer solstice perihelion simulations may affect annual-mean differences.

	Lo–Hi	WS–SS	Doubled CO_2
Surface albedo	−0.27 (−0.28)	0.31 (0.18)	0.61
Water vapor	−0.20 (−0.61)	0.19 (0.61)	4.02
Lapse rate	−0.90 (−0.12)	0.47 (−0.24)	−0.70
Cloud	−0.67 (0.14)	0.74 (0.15)	1.06
Total	−2.03 (−0.87)	1.72 (0.69)	4.99

that corresponds to the change in specific humidity that would result from ΔT according to the Clausius–Clapeyron relation with a fixed RH and a dynamic component resulting from changes in atmospheric eddies and circulation patterns.

In the Lo–Hi experiment, thermodynamic changes are characterized by increased water vapor in the tropics, where ΔT is positive, and decreased water vapor elsewhere, where ΔT is negative. Dynamic changes show an additional increase in tropical water vapor associated with an enhanced annual-mean Hadley circulation, with enhanced dry zones in regions of subtropical descent. Enhancement of the annual-mean Hadley circulation is consistent with the increased equator-to-pole insolation and temperature gradients, as previously found by Otto-Bliesner and Clement (2004) and Rind and Perlwitz (2004).

In the WS–SS experiment, thermodynamic changes dominate at higher latitudes, but dynamic changes are equally large in the tropics. These dynamic changes are primarily associated with changes in monsoons. Precipitation differences in the WS–SS experiment (Table 3) reveal diminished NH rainy seasons in North America, northern Africa, and Asia and enhanced SH rainy seasons in South America, southern Africa, and Australia. Changes in monsoon intensity affect the amount of water vapor transported into continental regions, with weakened NH monsoons transporting less water vapor into NH continents and strengthened SH monsoons transporting more. Strengthening and weakening of monsoons in response to precession forcing is a robust feature of both proxy (e.g., Fleitmann et al. 2007; Wang et al. 2008; Ziegler et al. 2010) and model (e.g., Prell and Kutzbach 1987; Tuenter et al. 2003; Wyrwoll et al. 2007) studies. Monsoon changes in the Lo–Hi experiment (not shown) are present, but comparatively small, mostly being characterized by weaker monsoons in most regions and equatorward shift of areas of maximum rainfall. The Australian monsoon shows only a small dependence on obliquity changes in the present WS–SS experiment, in contrast to larger variations modeled by Wyrwoll et al. (2007).

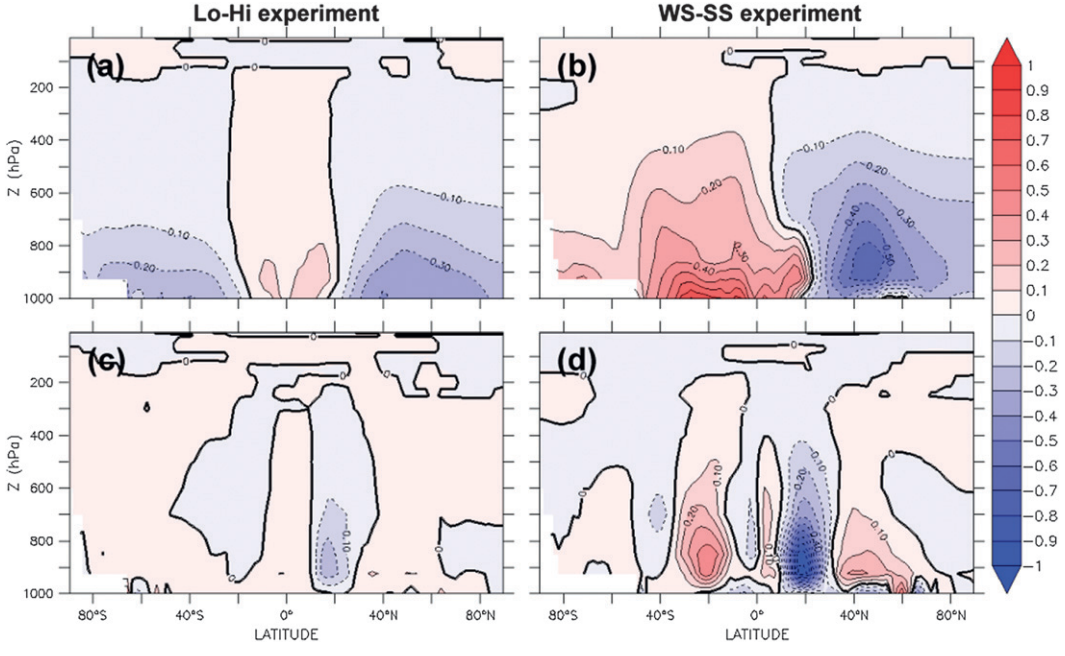

FIG. 4. Change in (a),(b) thermodynamic and (c),(d) dynamic components of specific humidity (g kg^{-1}) for the Lo–Hi and WS–SS experiments. The thermodynamic component is calculated as the change in specific humidity that would result from ΔT at a fixed RH. The dynamic component is approximated as the difference between the thermodynamic component and the actual change in specific humidity (Herweijer et al. 2005).

TABLE 3. Changes in summer precipitation (mm day^{-1}) for six monsoon regions in the WS–SS experiment. Values are calculated for respective summers in each hemisphere (June–August in the NH and December–February in the SH). Monsoon regions are defined as the land areas between the given latitudes and longitudes. Results show a weakening of NH monsoons and a strengthening of SH monsoons in the WS–SS experiment.

Monsoon	Change in summer precipitation (mm day^{-1})	Region	
		Latitudes	Longitudes
North American	−0.28	0°–40°N	130°–60°W
South American	2.64	40°S–0°	90°–30°W
North African	−2.37	0°–40°N	20°W–45°E
South African	2.55	40°S –0°	0°–60°E
Asian	−1.65	0°–40°N	60°–150°E
Australian	3.00	40°S–0°	100°–160°E

When considered in terms of global-mean climate response, the water vapor feedback is least important in these experiments. Despite strong regional effects, it is chiefly characterized by positive and negative effects of nearly equal magnitude. It accounts for only about 10% of the total global-mean ΔR_{net} in both Lo–Hi and WS–SS experiments (Table 2).

c. Lapse rate feedback

The ΔR_{net} from the lapse rate feedback is shown in Figs. 3e and 3f. The lapse rate feedback is related to changes in the vertical thermal structure of the atmosphere. At low latitudes, deep convection maintains a nearly moist adiabatic lapse rate, amplifying ΔT at higher altitudes through the transport of latent heat. At higher latitudes, where synoptic systems play a larger role and the lapse rate is not moist adiabatic, ΔT is generally smaller aloft relative to the surface (Bony et al. 2006).

In the Lo–Hi experiment, ΔR_{net} from the lapse rate feedback is mostly negative at higher latitudes and near zero in the tropics. This is partly consistent with the latitudinal nature of the response mentioned above: at higher latitudes the temperature decreases more at the surface than aloft. Seasonally, a large reversal occurs in the sign of the Arctic lapse rate feedback between NH summer and fall. The reduced Arctic stability during NH summer results from melting ice keeping the surface temperatures near freezing while temperatures cool aloft. This happens because of the influence of sea ice. Sea ice melting is reduced during NH summer but, because there is enough energy to melt sea ice in both cases, surface temperature stays near zero while temperatures cool aloft, leading to reduced atmospheric stability. Afterward, in NH fall, increased sea ice better insulates the surface air from the Arctic waters, allowing temperatures to plummet more quickly at the surface and resulting in increased atmospheric stability. Manabe and Stouffer (1980), Robock (1983), and Hall (2004) observe the same mechanism in increased CO_2 and altered solar constant experiments, noting that anomalous insolation largely impacts sea ice melt rather than ΔT in NH summer, while subsequent sea ice thickness anomalies affect ΔT through changes in ocean insulation in NH fall and winter. This dichotomy between the lapse rate feedback in Arctic summer and fall also influences local clouds, discussed in the next section. Additionally, the lapse rate feedback tends to be negatively correlated with the water vapor feedback, which partially counteracts its effects (Colman 2003; Bony et al. 2006).

In the WS–SS experiment, many of these same features are observed, but like the water vapor response, sign changes are more seasonal in nature. In the low latitudes, where the lapse rate is closer to moist adiabatic, the effect of the lapse rate feedback is generally positive when ΔT is negative and negative when ΔT is positive. In the Arctic, cooler summers lead to the same dichotomy of summer and fall lapse rates that was seen in the Lo–Hi experiment.

Of the four radiative feedbacks, the lapse rate feedback has among the largest effects in both the Lo–Hi and WS–SS experiments, resulting in a global-mean ΔR_{net} of $-0.90\,\text{W m}^{-2}$ for Lo–Hi and $+0.47\,\text{W m}^{-2}$ for WS–SS.

d. Cloud feedback

Figures 3g and 3h show ΔR_{net} from the cloud feedback in the Lo–Hi and WS–SS experiments. Because cloud feedback can affect both the SW and LW radiation, it is useful to view those effects separately (Fig. 5). In the Lo–Hi experiment, the effect of clouds is manifested most strongly in the SW component, with the LW effect being smaller and opposite at most latitudes. Outside of the tropics, the SW effect is dictated predominantly by changes in cloud liquid water content. Since cloud droplet concentration is held constant in the CM2.1 (Anderson et al. 2004), increased cloud liquid water results in an unchanged concentration of larger droplets, which increases cloud albedo. The modeled SW effect is also affected by increases in low-cloud fraction throughout much of the midlatitudes, especially over NH continental areas and the Southern Ocean (Fig. 6). The LW effects are mostly caused by changes in high clouds (not shown), with areas of positive LW ΔR_{net} generally being associated with increased high cloud fraction. An analysis of interannual variability in a preindustrial CM2.1 simulation reveals that, with the exception of over Greenland, Arctic cloud water content is positively correlated with stability in July (Fig. 7). This relationship

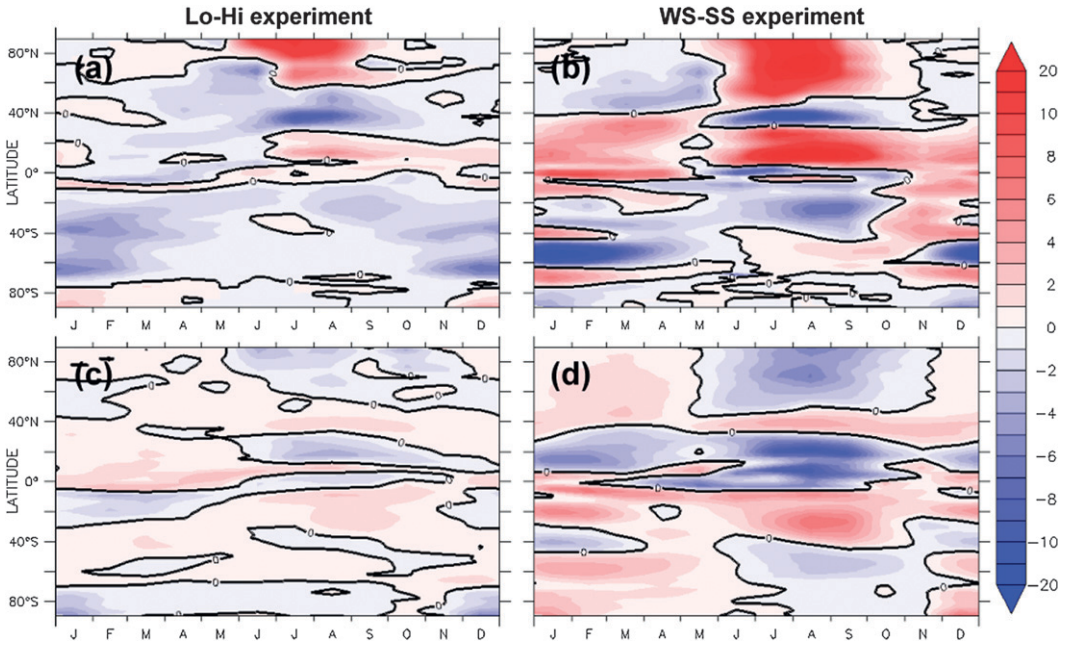

FIG. 5. Effect of the cloud feedback on zonal-mean net TOA radiation (W m^{-2}) broken down into (a),(b) SW and (c), (d) LW effects in the Lo–Hi and WS–SS experiments.

suggests that the decrease in Arctic cloud water content during NH summer is associated with the decreased stability during those months. In a more stable atmosphere, the inhibition of vertical mixing allows moisture to remain concentrated in the Arctic boundary layer, resulting in greater cloud water content at low levels. A decrease in stability is thus associated with a reduction in the water content of low clouds in the model. The cloud feedback accounts for about 33% of the global-mean ΔR_{net} in the Lo–Hi experiment. A more

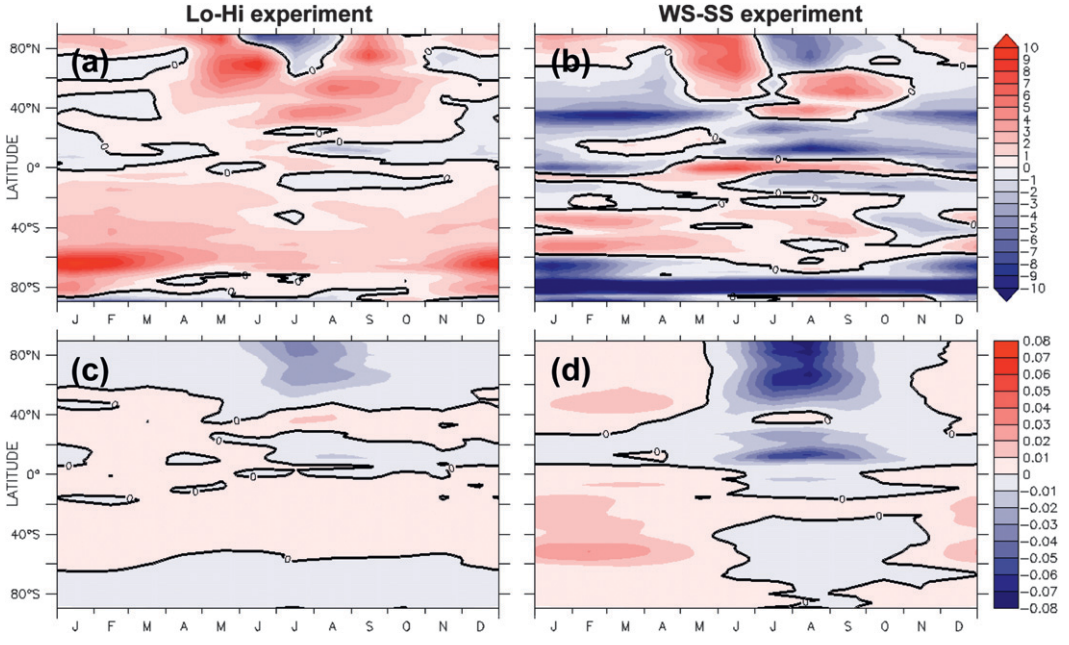

FIG. 6. Change in (a),(b) zonal-mean low-cloud sky fraction (%) and (c),(d) vertically integrated cloud water (kg m^{-2}) for the Lo–Hi and WS–SS experiments.

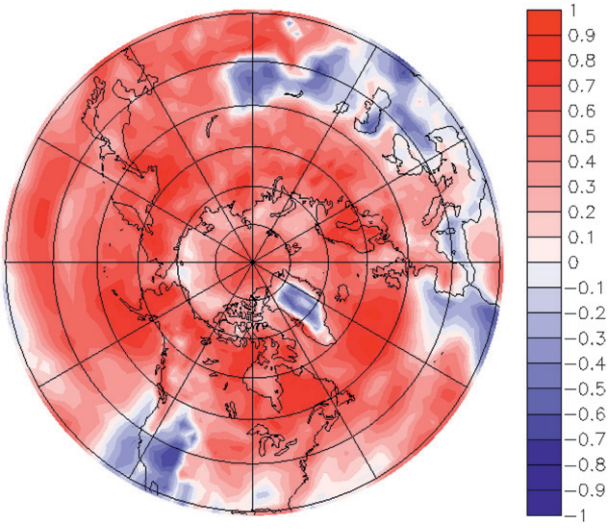

FIG. 7. Temporal correlation between cloud water content and stability for July at 30°–90°N. The correlation is computed using 100 Julys of a preindustrial simulation and shows how water content varies with stability during Arctic Julys.

detailed analysis of these cloud changes may be found in Mantsis et al. (2011).

The cloud feedback in the WS–SS experiment is more spatially complex and larger in magnitude than the Lo–Hi experiment, contributing over 40% of the global annual-mean ΔR_{net}. Annual-mean ΔR_{net} is positive over most oceanic regions with negative values generally confined to continental areas and limited oceanic areas such as the band of ocean between ~40° and 60°S. As in the Lo–Hi experiment, changes in ΔR_{net} from clouds primarily result from SW effects, with LW effects generally being opposite sign and smaller. The exception to this is near the equator, where changes in SW and LW are comparable due primarily to two mechanisms. First, weakened NH monsoons over northern Africa, India, and parts of China result in reduced cloud water content, ice content, and cloud fraction over those areas during NH summer. Strengthened SH monsoons over South America, southern Africa, and Australia have an approximately opposite effect in those regions. Of the monsoons, the North African monsoon has the largest impact on cloud feedback, resulting in an annual-mean ΔR_{net} over West Africa of more than $20\,\text{W m}^{-2}$. The second mechanism is the cooling of the eastern equatorial Pacific of over 2 K during NH summer, which is associated with increases in low clouds at the expense of mid- and high clouds. Unlike most of the other changes in cloud fraction, this is accompanied by little change in cloud water content and is simply a preferential increase in low clouds. Similar preferential changes in clouds may be seen in Clement et al. (2010). These cloud changes are not the primary cause of the eastern equatorial Pacific ΔT, but they contribute to ΔR_{net} by more than $-20\,\text{W m}^{-2}$ over much of the region during NH summer. A warming of the eastern equatorial Pacific during NH winter results in positive ΔR_{net} during that time.

By far the largest effect of clouds in the WS–SS experiment occurs in the NH high-latitude summer. Widespread decreases in cloud water content at latitudes poleward of 40°N in the WS–SS experiment likely result from decreased high-latitude summer stability. The associated reduction in cloud albedo, together with a decrease in low-cloud fraction over the Arctic and northern Atlantic and Pacific basins during July and August (Fig. 6), allows a larger percentage of SW radiation to the reach the surface. This results in a ΔR_{net} from the cloud feedback between +15 and $+20\,\text{W m}^{-2}$ in the NH high-latitude summer, partially counteracting the direct radiative forcing. In these experiments, clouds may be regarded as a negative feedback on orbital forcing in this region and will be discussed further in section 6.

Because clouds have long been considered one of the major sources of uncertainty in climate modeling, it is reasonable to wonder if the cloud responses described above may be model dependent, particularly given that much of the change comes from the effect of clouds on SW radiation. Soden and Vecchi (2011) analyzed doubled CO_2 experiments in 12 coupled AOGCMs and showed that while there is some spread among the models, they do agree on many characteristics of cloud feedback. A comparison of CM2.1 cloud feedbacks with the multimodel analysis of Soden and Vecchi (2011) indicates that the behavior of the GFDL CM2.1 is broadly consistent with other AOGCMs (Fig. 8). The main disagreement between models occurs in the relatively small area poleward of 80°N in the SW component. The general agreement between these models provides some confidence that the results obtained in the present orbital forcing experiments may not be model dependent.

e. *Total feedbacks*

The total effect of the surface albedo, water vapor, lapse rate, and cloud feedbacks is shown in Figs. 3i and 3j for the Lo–Hi and WS–SS experiments, respectively. In the Lo–Hi experiment, the feedbacks generally result in strongly negative ΔR_{net} at the mid- and high latitudes and a weakly positive ΔR_{net} at the low latitudes. This cools the mid- and high latitudes much more than it warms the low latitudes, contributing to the modeled temperature response. In the WS–SS experiment, ΔR_{net} is mostly positive from November to April, with a mix of

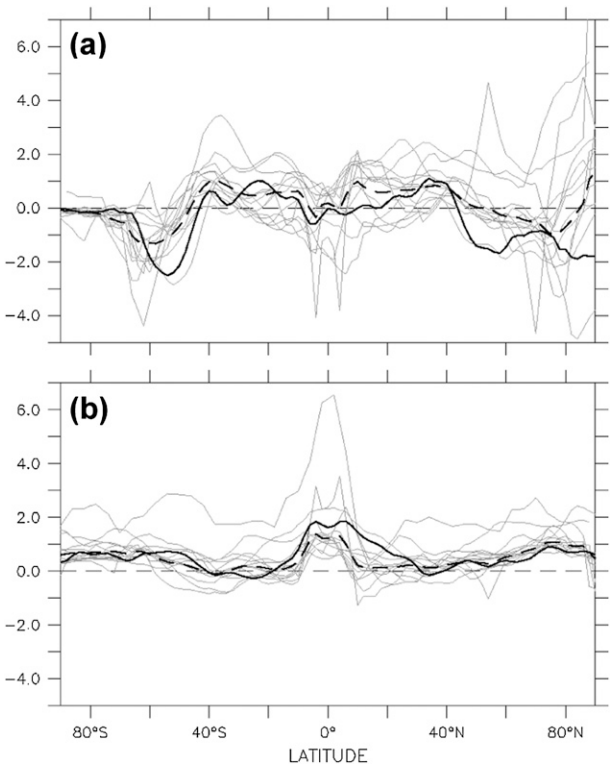

FIG. 8. Annual zonal-mean (a) SW and (b) LW cloud feedbacks ($W m^{-2} K^{-1}$) from the CM2.1 (solid black) and 13 other CMIP3 models in a doubled CO_2 run (gray). Also shown is the ensemble of the models (dashed black).

positive and negative ΔR_{net} during the rest of the year, contributing to the modeled annual-mean warming in the WS–SS experiment.

When looking at global annual-mean values, the lapse rate and cloud feedbacks contribute most strongly to the total ΔR_{net}, together accounting for over 70% of the total ΔR_{net} in each experiment (Table 2). Water vapor accounts for the smallest mean changes in the orbital experiments, which is in contrast to the doubled CO_2 experiment, where it is the most important by far, and the surface albedo feedback shows similar magnitude of effects in the two experiments despite vastly different forcings. Because obliquity and precession variations result in equal areas of positive and negative TOA insolation anomalies, the global-mean importance of each feedback becomes dependent on the spatial and temporal distribution of the forcing, the nonlinearities of each feedback's response to positive and negative forcing, and other large-scale mechanisms such as circulation and monsoons. It is worth noting that all four feedbacks work counter to the initial weak radiative forcing in both orbital experiments. Total ΔR_{net} from these fast radiative feedbacks is $-2.03\,W m^{-2}$ in the Lo–Hi experiment and $+1.72\,W m^{-2}$ in the WS–SS experiment, leading to ΔT of -0.5 K and $+0.6$ K, respectively. Even when given no global annual-mean insolation change, feedbacks can push the climate toward a colder (as in the Lo–Hi experiment) or warmer (as in the WS–SS experiment) state.

5. Comparison with feedbacks under doubled CO_2 forcing

To more fully understand the mechanisms responsible for feedbacks in the orbital experiments, feedbacks computed for the Lo–Hi and WS–SS experiments with the kernel method are compared with feedbacks estimated from the CM2.1 doubled CO_2 experiment. Three questions are posed: 1) To what extent are feedbacks in the orbital experiments consistent with those responding to doubled CO_2? 2) Can feedbacks be understood as a simple response to local ΔT, regardless of the type of forcing, or are spatially and seasonally dependent response mechanisms at play? 3) If these other mechanisms do produce some of the regional climate change, are they also important to the global-mean response?

To answer these questions, a calculation is performed to estimate the effect feedbacks would have if the relationship between each feedback and local ΔT was exactly the same in the orbital experiments as it is in the doubled CO_2 experiment. Stated more explicitly, these estimated feedbacks are calculated by dividing ΔR_{net} from doubled CO_2 feedbacks by the seasonally/spatially varying surface ΔT in the doubled CO_2 experiment to normalize for temperature, then multiplying them by the ΔT in each orbital experiment, as expressed below:

$$\text{estimated effect of feedback} = \delta F_{CO_2}\left(\frac{\Delta T_{orbital}}{\Delta T_{CO_2}}\right).$$

Values of ΔT_{CO_2} (not shown) are generally consistent with ΔT from other doubled CO_2 experiments, with a global-mean ΔT_{CO_2} of $+2.4$ K. We compare the actual effect of feedbacks in the orbital runs, calculated with the kernel method (Fig. 3), with the estimated effect of feedbacks as determined above (Fig. 9). If the actual and estimated figures were identical, it would imply that the effect of feedbacks on ΔR_{net} varied linearly with local surface ΔT in the same manner in both the doubled CO_2 and orbital experiments, and that the feedbacks depend only on the local temperature response. Differences between the actual and estimated response indicate a dependence on more complex response mechanisms. Global-mean values for the estimated feedbacks are given in parentheses in Table 2.

A shortcoming of this method is the overestimation of feedback effects in areas where ΔT_{CO_2} is near zero. To

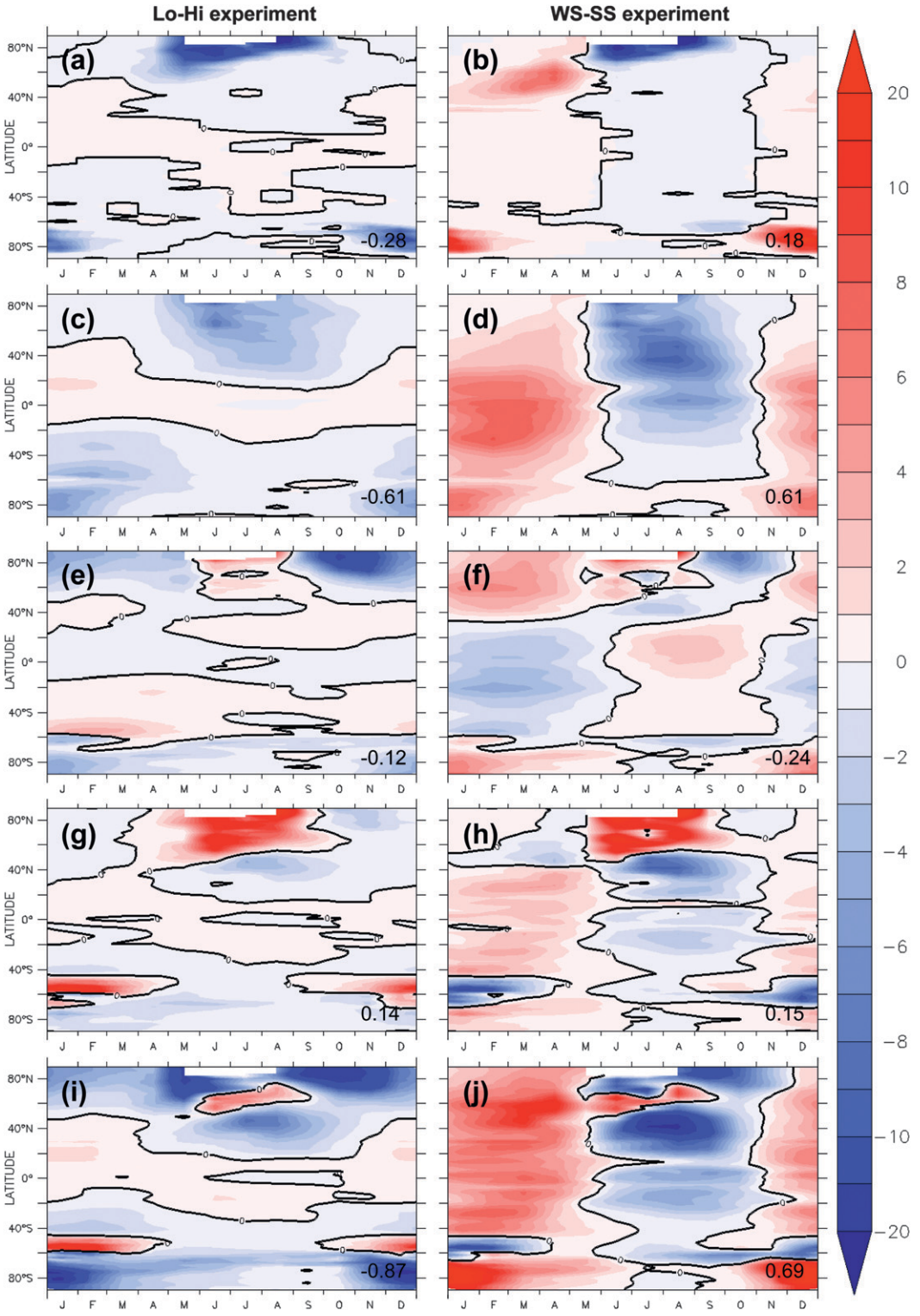

FIG. 9. Effect of feedbacks on zonal-mean ΔR_{net} (W m^{-2}) estimated as the product of the doubled CO_2 feedback and the ΔT in each orbital experiment. As in Fig. 3, plots are shown for ΔR_{net} caused by (a),(b) surface albedo, (c),(d) water vapor, (e),(f) lapse rate, (g),(h) clouds, and (i),(j) the sum of all four for the Lo–Hi and WS–SS experiments. Positive values represent increased net downward radiation. Global-mean values (W m^{-2}) are given in the bottom right of each panel.

account for this, areas where ΔT_{CO_2} is between -0.5 and $+0.5$ K have been masked out. However, the estimate is still disproportionately affected by areas of low ΔT_{CO_2}, so this section will focus primarily on differences in sign, not magnitude, in the comparison of the actual (Fig. 3) and estimated (Fig. 9) effect of feedbacks.

a. Lo–Hi experiment

Of the four feedbacks in the Lo–Hi experiment, the surface albedo feedback shows the strongest similarities between the actual and estimated response, suggesting that changes in snow and sea ice are primarily associated with local ΔT and do not rely heavily on other mechanisms. While this is perhaps not surprising, it is interesting to note that the actual and estimated responses are similar, despite the opposite signs of high-latitude ΔT in the Lo–Hi and CO_2 experiments.

In the remaining feedbacks, differences are apparent in the mid- to high latitudes during summer in both hemispheres. The high-latitude changes stem from relatively low ΔT_{CO_2} in the Southern Ocean and northern Atlantic during their respective summers, where changes in ocean circulation tend to reduce local warming in global warming experiments (Stouffer et al. 2006) and in the parts of Canada and Russia during NH summer, where ΔT_{CO_2} is low because of increased precipitation in the doubled CO_2 experiment (Wetherald 2010). Increased precipitation throughout the year in these NH high-latitude continental regions makes the soil wetter, allowing increased evaporation during NH summer. This decrease in the Bowen ratio diminishes local warming. Because ΔT in the orbital experiments is not affected in the same way in these regions, differences arise between the actual and estimated feedback responses.

In the water vapor feedback, the calculated effect of the water vapor feedback is larger at the equator and smaller in the North African and Asian monsoon regions than in the estimation. This difference is caused by the enhanced Hadley circulation and a slight weakening of those monsoons in the Lo–Hi experiment, both of which rely more on the latitudinal temperature gradient than local ΔT alone. Monsoon changes also lead to differences in the cloud feedback, as weaker NH monsoons result in local decreases in summer clouds. These cloud feedbacks are not well reproduced in the estimated response.

Outside of these regional variations, several wider-scale differences should be addressed. In particular, the calculated effects of the lapse rate and cloud feedbacks are more negative than in the estimate, and the effect of the water vapor feedback is more positive (Table 2). One hypothesis to explain these differences involves the transport of moist static energy (MSE) by the mean meridional circulation. In the Lo–Hi experiment, increases in insolation at low latitudes produce positive MSE anomalies through increases in surface air temperature and specific humidity. Decreases in insolation at high latitudes have the opposite effect. From a Lagrangian perspective, the mean meridional circulation transports low-latitude air upward and poleward, while air at the poles is transported downward and equatorward. This circulation should transport positive MSE anomalies poleward in the upper troposphere and negative MSE anomalies equatorward near the surface. This differential transport should have the effect of stabilizing the atmosphere in the Lo–Hi experiment and affecting radiative feedbacks in three important ways: 1) A decreased lapse rate emits more LW radiation to space, cooling the climate; 2) a more stable atmosphere sustains additional water vapor at height, increasing the greenhouse effect and partially offsetting the primary radiative effect of a decreased lapse rate; and 3) a more stable atmosphere encourages increased cloud water (Fig. 7), reflecting more insolation back to space. Thus, despite potential changes in water vapor, the export of high-latitude air with reduced MSE by the mean meridional circulation may be responsible for pushing the Lo–Hi experiment toward a colder global-mean climate. This would allow regions of negative ΔT to be sustained equatorward of the regions of negative insolation change, as seen between approximately 20° and 40° latitude in both hemispheres in the Lo–Hi experiment.

Outside of these important differences, however, many aspects of the feedback responses remain relatively consistent between the Lo–Hi and CO_2 experiments. The sign of the surface albedo and water vapor feedbacks is consistent over most regions, as are the lapse rate and cloud feedbacks outside of the midlatitudes, suggesting that many aspects of the feedbacks depend upon the local temperature change and are relatively insensitive to the global distribution and type of forcing. Notably, the dichotomy between the Arctic summer and fall lapse rate responses in the Lo–Hi experiment is well reproduced in the estimated feedback response, reinforcing the notion that this feature is a robust model response largely dependent on local, rather than global, processes.

This comparison between actual and estimated feedbacks suggests that many aspects of feedbacks are a direct response to local ΔT, but some aspects depend on changes in atmospheric circulation. This is especially apparent when comparing the total effect of feedbacks (Figs. 3i, 9i), which show large-scale similarities as well as some important differences. Table 2 lists global-mean values of ΔR_{net} for both the actual and estimated response. The surface albedo and water vapor responses

are relatively similar, but the larger differences in the lapse rate and cloud responses indicate complexities in the relationship between feedbacks and the seasonal and latitudinal pattern of temperature change.

b. WS–SS experiment

Comparing the actual and estimated responses in the WS–SS experiment reveal large-scale similarities, but, as in the Lo–Hi experiment, important differences become apparent as well. For the water vapor feedback, the greatest differences occur at low latitudes, mostly corresponding to monsoonal changes, which are much larger in the WS–SS experiment than the doubled CO_2 experiment. These large monsoonal changes in the WS–SS experiment point to the importance of the seasonality of the forcing. Because the thermal inertia of the ocean allows the climate system to maintain a memory of forcing in earlier seasons, previous seasonal changes may impact later climate response. It is important to note, however, that while NH and SH monsoons produce changes in the water vapor feedback that are of the opposite sign, these anomalies are not of equal magnitude, making the actual ΔR_{net} from the water vapor feedback $+0.19\,\text{W m}^{-2}$, while the estimated one is $+0.61\,\text{W m}^{-2}$. Some of this stems from the fact that changes in the North African monsoon are more pronounced than changes in other monsoons, significantly decreasing the water vapor over northern Africa.

Monsoon changes also explain some of the differences in the lapse rate and cloud feedbacks. In the lower latitudes, less convectively active NH monsoons transport less latent heat aloft, increasing the lapse rate over northern Africa and the Indian subcontinent. The SH monsoons have the opposite effect over South America, southern Africa, and Australia during SH summer. Monsoonal changes also reduce cloud water content and cloud fraction over NH monsoon regions and increase them over SH monsoon regions. These changes, as well as the response of clouds to seasonal temperature anomalies in the eastern equatorial Pacific, are not well represented in the estimated response. This is apparent when comparing the total effect of feedbacks (Figs. 3j, 9j), again pointing toward the importance of seasonal variations in determining parts of the feedback response.

Taking a step back, Table 2 shows that the latitudinal- and seasonal-dependent response mechanisms outlined above are important not just to aspects of local ΔR_{net} but also to global ΔR_{net}. Therefore, the questions posed at the beginning of this section may be answered as follows: 1) There are many large-scale similarities between the actual and estimated effect of the feedbacks, but also crucial differences. 2) Important parts of the feedback response cannot be understood as a simple response to local ΔT. 3) Changes in systems such as the Hadley circulation and monsoons are important to the global-mean climate response.

6. Potential effect of feedbacks on expansion of NH ice sheets

According to orbital theory, low obliquity and perihelion at NH winter solstice (which are simulated separately in Lo–Hi and WS–SS) should promote NH ice sheet growth by allowing high-latitude snow to survive through cooler summers. Although the current experiments cannot explicitly address the slow feedbacks that are instrumental in amplifying the climate response to orbital changes because of the absence of dynamic ice sheets and biogeochemistry in CM2.1, the fast radiative feedbacks can be evaluated to see whether they encourage high-latitude NH perennial snow cover in these experiments or not.

Both Lo–Hi and WS–SS result in high-latitude cooling during the NH summer, with Lo–Hi additionally cooling at high latitudes year round (Fig. 2). Spatially, the NH high-latitude summer ΔT is negative almost everywhere in both experiments (Figs. 10a,b, shading), though the WS–SS experiment has ΔT near zero over northern ocean areas. Some of this pattern may be attributed to the summer cloud feedback (Figs. 10a,b, contours), which contributes positive ΔR_{net} over high-latitude ocean regions and some continental regions in both experiments. The total effect of feedbacks (not shown) has the same sign as the cloud feedbacks over most latitudes, enhancing cooling in some regions while diminishing it in others.

The NH high-latitude summer WS–SS cloud feedback constitutes one of the largest feedbacks seen anywhere in the orbital experiments and, as previously stated, involves widespread decreases in cloud water content over the majority of regions poleward of approximately 40°N associated with decreased high-latitude summer stability. Together with a decrease in low-cloud fraction over the Arctic and northern ocean basins during July and August (Fig. 6), this decrease in cloud water reduces cloud albedo and allows a higher percentage of SW radiation to reach the surface. The region of positive ΔR_{net} from the cloud feedback extends over parts of northern Canada including Baffin Island, which remains one of the most likely locations for past initiations of the Laurentide Ice Sheet (Clark et al. 1993). This suggests that the cloud feedback could partially counteract changes in summer insolation at or near these regions at times when the orbital configuration is favorable for ice sheet expansion.

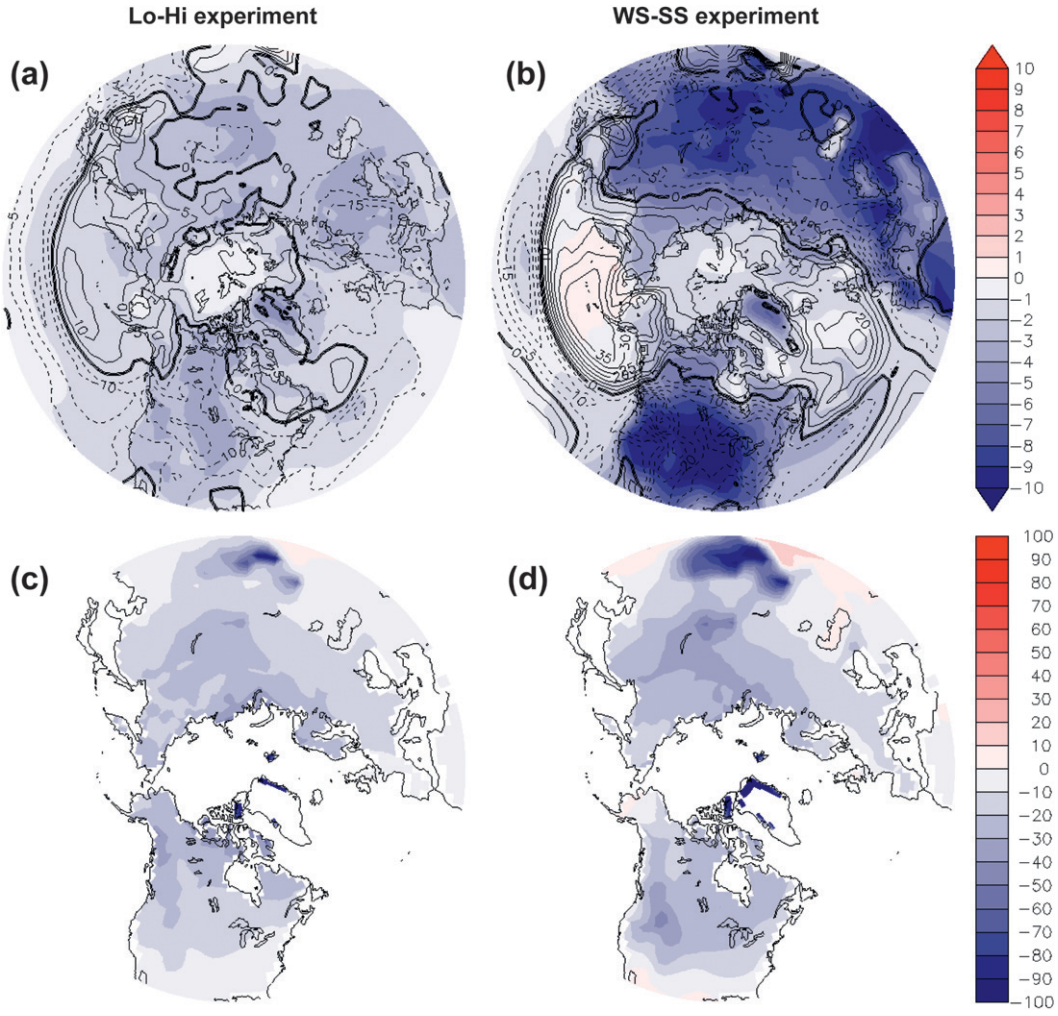

FIG. 10. (top) Mean June–August ΔT poleward of 30°N in the (a) Lo–Hi and (b) WS–SS experiments (K; shaded). Contours are the ΔR_{net} from the mean June–August cloud radiative feedback ($W\,m^{-2}$). (bottom) Percent change in annual melting degree-days over land for (c) Lo–Hi and (d) WS–SS. Melting degree-days are calculated from climatological monthly values as the product of monthly temperature (for months that are above zero, in °C) and number of days per month. White areas over Greenland remain below freezing year round, so they have no melting degree-days in either simulation.

However, despite the decreases in insolation and continental temperature in both experiments, neither experiment shows a widespread increase in perennial snow cover, which would be the precursor to ice sheets. Perennial snow cover remains confined to Greenland and Antarctica, with the sole exception of a single point over the Himalayas in the WS–SS experiment, which maintains its snow throughout the cooler summer. An analysis of melting degree-days, which indicate whether snowmelt would increase or decrease over the course of the year, shows that these experiments are still in agreement with orbital theory. Figures 10c and 10d show that melting degree-days are reduced over almost all continental regions poleward of 30°N. Because continental temperature can drop significantly below zero in winter, melting degree-days are more affected by summer ΔT, which is negative in both experiments, than by winter ΔT, which is negative in the Lo–Hi experiment but positive in the WS–SS experiment. These reductions in melting degree-days should allow snow to remain on the ground later in the melt season in both experiments.

Large-scale increases in perennial snow cover are not expected in these experiments for several reasons: First, the present experiments model low obliquity and NH winter solstice perihelion forcing separately, while orbital theory suggests that both should be present to start glaciations. Second, GFDL CM2.1 lacks the fine resolution required to resolve the tall mountain peaks where glaciations likely begin. Third, when comparing a modern run from GFDL CM2.1 against data from the

Climatic Research Unit, version 2.1 (CRU v.2.1), temperature dataset (Mitchell and Jones 2005), GFDL CM2.1 displays a warm bias of several degrees over northern Canada and parts of northern Russia during NH summer. This warm bias increases the drop in temperature needed to promote permanent snow cover in the CM2.1, even if the first two reasons listed above are ignored.

As a final note, an open question remains regarding how feedbacks may change as ice sheets grow. Changes in surface type and elevation, both of which will happen with expanding ice sheets, could have significant effects on feedbacks. Snow feedbacks, which can be pronounced over dark surfaces such as forests and grasslands, would be much weaker over ice sheets, changing the regional characteristics of the surface albedo feedback. The lapse rate feedback will be affected by the much cooler surface temperatures. Higher topography associated with ice sheet growth may lead to a southward displacement of the NH winter jet stream (Clark et al. 1999). Such changes in the atmospheric circulation and topography may influence the cloud feedback. Because of the complexity of these potential responses, feedbacks that initially discourage or promote high-latitude cooling may change with the growth of ice sheets. While this topic deserves further research, analysis of those potential responses is beyond the scope of the present experiments.

7. Summary and conclusions

The role of orbital cycles in influencing past climate variations has been the subject of much discussion over the past decades, and understanding the role of feedbacks in amplifying or damping that response remains an intriguing question. To isolate and explore these feedbacks, this study forced an AOGCM with idealized orbital forcings, where obliquity and longitude of the perihelion are varied without the competing effects of changes in ice sheets and atmospheric composition. The effects of feedbacks in these simulations were analyzed and compared with those estimated from a doubled CO_2 experiment to determine whether feedbacks behave consistently under orbital and anthropogenic forcing. From the results, the following statements may be made:

1) Global-mean climate change can result from a simple redistribution of insolation, even when global-mean insolation change is zero and radiative forcing is small, because of the influence of radiative feedbacks. Furthermore, ΔT does not have to be the same sign as the radiative forcing, either locally or globally, if the effects of feedbacks are sufficient to overwhelm the direct radiative forcing.
2) The relative importance of each feedback to the global-mean climate response is contingent on the temporal and spatial distribution of the forcing. While the water vapor feedback results in the largest global-mean ΔR_{net} in the doubled CO_2 experiment (Table 2), it provides the smallest global-mean ΔR_{net} in both orbital experiments. The lapse rate and cloud feedbacks prove most important in both orbital experiments, together accounting for over 70% of the global-mean ΔR_{net} from feedbacks.
3) While many aspects of the feedbacks may be considered a simple response to local ΔT, some are not, especially in the water vapor, lapse rate, and cloud feedbacks. Circulation changes, which are largely dependent on the seasonal and spatial patterns of forcing, affect regional feedbacks in important ways. Monsoon circulations are especially important, playing a large role in influencing WS–SS feedbacks and a smaller role in influencing Lo–Hi feedbacks.
4) Vertical variations in the meridional transport of MSE anomalies may play a role in extending the reach of local climate anomalies to more distant areas. In the Lo–Hi experiment, increases in MSE in the tropics may be transported poleward at altitude while negative MSE anomalies from the high latitudes are transported equatorward near the surface, increasing the large-scale stability of the atmosphere and encouraging global-mean cooling through impacts on the lapse rate and cloud feedbacks.
5) Cloud feedbacks partially counteract changes in summer insolation over some NH high-latitude ocean and continental regions during times most favorable for ice sheet expansion. However, it is unclear how clouds would react to ice sheet expansion or reduction as the CM2.1 lacks dynamic ice sheets.

These results emphasize the significant role of radiative feedbacks in shaping orbitally forced climate change. Undoubtedly, feedbacks have played a large role in influencing climate in the past and will continue to do so in the coming century. Better understanding of how these feedbacks operate under a variety of forcings may help us understand what role feedbacks will play in the future.

Acknowledgments. This research was supported by the Paleo Perspectives on Climate Change program of the National Science Foundation (Grant ATM0902735). The authors would like to extend their thanks to F. Zeng and J. Krasting for their help in conducting these simulations; B. Soden for use of the radiative kernels and CMIP3 calculations; D. Pollard for help with the calendar conversion; V. Ghate, J. Kay, and N. Barton for their cloud expertise; and the NOAA Geophysical Fluid

Dynamics Laboratory at Princeton for use of their computing resources. Additionally, we thank two anonymous reviewers for their useful comments.

REFERENCES

Anderson, J. L., and Coauthors, 2004: The new GFDL global atmosphere and land model AM2–LM2: Evaluation with prescribed SST simulations. *J. Climate,* **17,** 4641–4673.

Berger, A., and M. F. Loutre, 1991: Insolation values for the climate of the last 10 million years. *Quat. Sci. Rev.,* **10,** 297–317.

Bony, S., and Coauthors, 2006: How well do we understand and evaluate climate change feedback processes? *J. Climate,* **19,** 3445–3482.

Chen, G.-S., J. E. Kutzbach, R. Gallimore, and Z. Liu, 2010: Calendar effect on phase study in paleoclimate transient simulation with orbital forcing. *Climate Dyn.,* **37,** 1949–1960, doi:10.1007/s00382-010-0944-6.

Clark, P. U., and Coauthors, 1993: Initiation and development of the Laurentide and Cordilleran ice sheets following the last interglaciation. *Quat. Sci. Rev.,* **12,** 79–114, doi:10.1016/0277-3791(93)90011-A.

——, R. B. Alley, and D. Pollard, 1999: Northern Hemisphere ice-sheet influences on global climate change. *Science,* **286,** 1104–1111, doi:10.1126/science.286.5442.1104.

Clement, A. C., A. Hall, and A. J. Broccoli, 2004: The importance of precessional signals in the tropical climate. *Climate Dyn.,* **22,** 327–341, doi:10.1007/s00382-003-0375-8.

——, R. Burgman, and J. R. Norris, 2010: Response to comment on ''Observational and model evidence for positive low-level cloud feedback.'' *Science,* **329,** 277, doi:10.1126/science.1187667.

Colman, R., 2003: A comparison of climate feedbacks in general circulation models. *Climate Dyn.,* **20,** 865–873, doi:10.1007/s00382-003-0310-z.

Delworth, T. L., and Coauthors, 2006: GFDL's CM2 global coupled climate models. Part I: Formulation and simulation characteristics. *J. Climate,* **19,** 643–674.

Fleitmann, D., and Coauthors, 2007: Holocene ITCZ and Indian monsoon dynamics recorded in stalagmites from Oman and Yemen (Socotra). *Quat. Sci. Rev.,* **26,** 170–188, doi:10.1016/j.quascirev.2006.04.012.

Hall, A., 2004: The role of surface albedo feedback in climate. *J. Climate,* **17,** 1550–1568.

——, A. C. Clement, D. W. J. Thompson, A. J. Broccoli, and C. S. Jackson, 2005: The importance of atmospheric dynamics in the Northern Hemisphere wintertime climate response to changes in the earth's orbit. *J. Climate,* **18,** 1315–1325.

Hays, J. D., J. Imbrie, and N. J. Shackleton, 1976: Variations in the earth's orbit: Pacemaker of the ice ages. *Science,* **194,** 1121–1132.

Herweijer, C., R. Seager, M. Winton, and A. Clement, 2005: Why ocean heat transport warms the global mean climate. *Tellus,* **57A,** 662–675.

Huybers, P., 2006: Early Pleistocene glacial cycles and the integrated summer insolation forcing. *Science,* **313,** 508–511, doi:10.1126/science.1125249.

——, and E. Tziperman, 2008: Integrated summer insolation forcing and 40,000-year glacial cycles: The perspective from an ice-sheet/energy-balance model. *Paleoceanography,* **23,** PA1208, doi:10.1029/2007PA001463.

Imbrie, J., and Coauthors, 1993: On the structure and origin of major glaciations cycles 2. The 100,000-year cycle. *Paleoceanography,* **8,** 699–735.

Jackson, C. S., and A. J. Broccoli, 2003: Orbital forcing of Arctic climate: Mechanisms of climate response and implications for continental glaciations. *Climate Dyn.,* **21,** 539–557, doi:10.1007/s00382-003-0351-3.

Joussaume, S., and P. Braconnot, 1997: Sensitivity of paleoclimate simulation results to season definitions. *J. Geophys. Res.,* **102** (D2), 1943–1956.

Jouzel, J., and Coauthors, 2007: Orbital and millennial Antarctic climate variability over the past 800,000 years. *Science,* **317,** 793–796, doi:10.1126/science.1141038.

Khodri, M., M. A. Cane, G. Kukla, J. Gavin, and P. Braconnot, 2005: The impact of precession changes on the Arctic climate during the last interglacial–glacial transition. *Earth Planet. Sci. Lett.,* **236,** 285–304, doi:10.1016/j.epsl.2005.05.011.

Lee, S.-Y., and C. J. Poulsen, 2005: Tropical Pacific climate response to obliquity forcing in the Pleistocene. *Paleoceanography,* **20,** PA4010, doi:10.1029/2005PA001161.

——, and ——, 2008: Amplification of obliquity forcing through mean annual and seasonal atmospheric feedbacks. *Climate Past,* **4,** 515–534, doi:10.5194/cpd-4-515-2008.

Manabe, S., and R. J. Stouffer, 1980: Sensitivity of a global climate model to an increase of CO_2 concentrations in the atmosphere. *J. Geophys. Res.,* **85** (C10), 5529–5554.

Mantsis, D. F., A. C. Clement, A. J. Broccoli, and M. P. Erb, 2011: Climate feedbacks in response to changes in obliquity. *J. Climate,* **24,** 2830–2845.

Meehl, G. A., C. Covey, T. Delworth, M. Latif, B. McAvaney, J. F. B. Mitchell, R. J. Stouffer, and K. E. Taylor, 2007: The WCRP CMIP3 multimodel dataset: A new era in climate change research. *Bull. Amer. Meteor. Soc.,* **88,** 1383–1394.

Milankovitch, M., 1941: *Kanon der Erdbestrahlung und seine Anwendung auf das Eiszeitenproblem* (*Canon of Insolation and the Ice-Age Problem*). Royal Serbian Academy, Special Publication, Vol. 133, 633 pp.

Mitchell, T. D., and P. D. Jones, 2005: An improved method of constructing a database of monthly climate observations and associated high-resolution grids. *Int. J. Climatol.,* **25,** 693–712, doi:10.1002/joc.1181.

Otto-Bliesner, B., and A. C. Clement, 2004: The sensitivity of the Hadley circulation to past and future forcings in two climate models. *The Hadley Circulation: Present, Past and Future,* H. F. Diaz and R. S. Bradley, Eds., Advances in Global Change Research Series, Vol. 21, Springer Verlag, 437–464.

Petit, J. R., and Coauthors, 1999: Climate and atmospheric history of the past 420,000 years from the Vostok ice core, Antarctica. *Nature,* **399,** 429–436.

Phillipps, P. J., and I. M. Held, 1994: The response to orbital perturbations in an atmospheric model coupled to a slab ocean. *J. Climate,* **7,** 767–782.

Pollard, D., and D. B. Reusch, 2002: A calendar conversion method for monthly mean paleoclimate model output with orbital forcing. *J. Geophys. Res.,* **107,** 4615, doi:10.1029/2002JD002126.

Prell, W. L., and J. E. Kutzbach, 1987: Monsoon variability over the past 150,000 years. *J. Geophys. Res.,* **92** (D7), 8411–8425.

Ramaswamy, V., and Coauthors, 2001: Radiative forcing of climate change. *Climate Change 2001: The Scientific Basis,* J. T. Houghton et al., Eds., Cambridge University Press, 349–416.

Raymo, M. E., and K. Nisancioglu, 2003: The 41 kyr world: Milankovitch's other unsolved mystery. *Paleoceanography,* **18,** 1011, doi:10.1029/2002PA000791.

Reichler, T., and J. Kim, 2008: How well do coupled models simulate today's climate? *Bull. Amer. Meteor. Soc.,* **89,** 303–311.

Rind, D., and J. Perlwitz, 2004: The response of the Hadley circulation to climate changes, past and future. *The Hadley Circulation: Present, Past and Future,* H. F. Diaz and R. S. Bradley, Eds., Advances in Global Change Research Series, Vol. 21, Springer Verlag, 399–435.

Robock, A., 1983: Ice and snow feedbacks and the latitudinal and seasonal distribution of climate sensitivity. *J. Atmos. Sci.,* **40,** 986–997.

Soden, B. J., and I. M. Held, 2006: An assessment of climate feedbacks in coupled ocean–atmosphere models. *J. Climate,* **19,** 3354–3360.

——, and G. A. Vecchi, 2011: The vertical distribution of cloud feedback in coupled ocean-atmosphere models. *Geophys. Res. Lett.,* **38,** L12704, doi:10.1029/2011GL047632.

——, A. J. Broccoli, and R. S. Hemler, 2004: On the use of cloud forcing to estimate cloud feedback. *J. Climate,* **17,** 3661–3665.

——, I. Held, R. Colman, K. M. Shell, J. T. Kiehl, and C. A. Shields, 2008: Quantifying climate feedbacks using radiative kernels. *J. Climate,* **21,** 3504–3520.

Stouffer, R. J., and Coauthors, 2006: GFDL's CM2 global coupled climate models. Part IV: Idealized climate response. *J. Climate,* **19,** 723–740.

Timm, O., A. Timmerman, A. Abe-Ouchi, F. Saito, and T. Segawa, 2008: On the definition of seasons in paleoclimate simulations with orbital forcing. *Paleoceanography,* **23,** PA2221, doi:10.1029/2007PA001461.

Timmermann, A., S. J. Lorenz, S.-I. An, A. C. Clement, and S.-P. Xie, 2007: The effect of orbital forcing on the mean climate and variability of the tropical Pacific. *J. Climate,* **20,** 4147–4159.

Tuenter, E., S. L. Weber, F. J. Hilgen, and L. J. Lourens, 2003: The response of the African summer monsoon to remote and local forcing due to precession and obliquity. *Global Planet. Change,* **36,** 219–235, doi:10.1016/S0921-8181(02)00196-0.

——, ——, ——, and ——, 2005a: Sea-ice feedbacks on the climatic response to precession and obliquity forcing. *Geophys. Res. Lett.,* **32,** L24704, doi:10.1029/2005GL024122.

——, ——, ——, ——, and A. Ganopolski, 2005b: Simulation of climate phase lags in response to precession and obliquity forcing and the role of vegetation. *Climate Dyn.,* **24,** 279–295, doi:10.1007/s00382-004-0490-1.

Wang, Y., and Coauthors, 2008: Millennial- and orbital-scale changes in the East Asian monsoon over the past 224,000 years. *Nature,* **451,** 1090–1093, doi:10.1038/nature06692.

Wetherald, R. T., 2010: Changes of time mean state and variability of hydrology in response to a doubling and quadrupling of CO_2. *Climatic Change,* **102,** 651–670, doi:10.1007/s10584-009-9701-4.

Wyrwoll, K.-H., Z. Liu, G. Chen, J. E. Kutzbach, and X. Liu, 2007: Sensitivity of the Australian summer monsoon to tilt and precession forcing. *Quat. Sci. Rev.,* **26,** 3043–3057, doi:10.1016/j.quascirev.2007.06.026.

Yoshimori, M., and A. J. Broccoli, 2008: Equilibrium response of an atmosphere–mixed layer ocean model to different radiative forcing agents: Global and zonal mean response. *J. Climate,* **21,** 4399–4423.

Ziegler, M., E. Tuenter, and L. J. Lourens, 2010: The precession phase of the boreal summer monsoon as viewed from the eastern Mediterranean (ODP site 968). *Quat. Sci. Rev.,* **29,** 1481–1490, doi:10.1016/j.quascirev.2010.03.011.